Journal of Industrial and Engineering Chemistry xxx (xxxx) xxx

Contents lists available at ScienceDirect

Journal of Industrial and Engineering Chemistry

journal homepage: www.elsevier.com/locate/jiec

Introducing ZnMgO quantum dots to enhance optoelectrical characteristics of organic photovoltaics via light downconversion

Hyoung Seok Lee, Chang Ho Jung, Doo Kyung Moon *

Nano and Information Materials (NIMs) Laboratory, Department of Chemical Engineering, Konkuk University, 120 Neungdong-ro, Gwangjin-gu, Seoul 05029, Republic of Korea

ARTICLE INFO

Keywords:
Organic photovoltaics
Electron transport layer
Quantum dots
Light downconversion
Optoelectrical properties

ABSTRACT

In this study, we developed organic photovoltaics (OPVs) with a photoactive layer based on the bulk heterojunction structure of the high-performance polymer PM6 and nonfullerene acceptor BTP-eC9. Zinc magnesium oxide (ZnMgO) quantum dots (QDs) were introduced into a zinc oxide sol–gel solution as the electron transport layer. The ZnMgO QDs absorb ultraviolet (UV) light and emit visible light (400–700 nm). The absorption area and external quantum efficiency of the fabricated OPV device were enhanced by converting UV light into visible light. Accordingly, the short-circuit current density and fill factor of the OPVs increased from 24.8 to 25.3 mA cm^{-2} and from 74.0 % to 74.8 %, respectively, and as a result, the power conversion efficiency of the OPVs increased from 15.1 % to 15.7 %. The absorption and photoluminescence emission and the particle size of the synthesized ZnMgO QDs were determined using UV–visible spectroscopy, photoluminescence spectroscopy, and high-resolution transmission electron microscopy.

Introduction

A recent trend in energy research has been to use photovoltaics to address climate change and global warming.[1–3] There are lots of photovoltaic classified by active materials, such as silicon, pervskite, organic materials, etc.[4–6] Organic photovoltaics (OPVs) in particular have been studied for decades owing to their low weight, ease of processing, and transparency to visible light.[7–10].

An OPV comprises a multilayer structure with a photoactive layer and an interlayer between a transparent conductive oxide and a metal electrode. The photoactive layer comprises a bulk heterojunction (BHJ) composed of electron donors and acceptors. The main principle of an OPV is the photovoltaic effect that converts solar energy into electrical energy. When incident solar light irradiates the photoactive layer, the electron donors and acceptors form charged carriers and excitons. Subsequently, the excitons are transported to the two electrodes of the OPV via charge dissociation, extraction, and transport. The light absorption level of the photoactive layer is the most crucial factor determining its power conversion efficiency (PCE).[11–13].

Numerous researchers have investigated the synthesis of photoactive materials and their different combinations toward enhancing their performance.[14–23] Since Jianhui Hou et al. and Yingping Zou et al. developed poly[(2,6-(4,8-bis(5-(2-ethylhexyl-3-fluoro)thiophen-2-yl)-benzo[1,2-b:4,5-b']dithiophene))-alt-(5,5-(1′,3′-di-2-thienyl-5′,7′-bis(2-ethylhexyl)benzo- [1′,2′-c:4′,5′-c']dithiophene-4,8-dione)] (PM6) and 2,2′-((2Z,2′Z)-((12,13-bis(2-ethylhexyl)-3,9-diundecyl-12,13-dihydro-[1,2,5]thiadiazolo[3,4-e]thieno[2″,3″:4′,5′]thieno[2′,3′:4,5]- pyrrolo [3,2-g]thieno[2′,3′:4,5]thieno[3,2-b]indole-2,10-diyl)bis(methanylylidene))bis(5,6-difluoro-3-oxo-2,3-dihydro-1H-indene-2,1-diylidene))-dimalononitrile (Y6), the PCE of OPVs has been considerably enhanced.[24–27].

The interlayer between an OPV's photoactive layer and electrode is essential because it assists charge transport, energy-level alignment, and light absorbance.[28] Thus, the performance of an OPV that does not have an interlayer will be considerably poor.

The interlayers of OPVs function as electron transport layers (ETLs) and hole transport layers (HTLs). Generally, zinc oxide (ZnO) and N,N'-Bis{3-[3-(Dimethylamino)propy-lamino]propyl}perylene-3,4,9,10-tetracarboxylic diimide (PDINN) are used as the ETLs, while poly(3,4-ethylenedioxythiophene)-polystyrene sulfonate (PEDOT:PSS) and molybdenum oxide (MoO_3) are used as the HTLs. Zinc oxide has been used as an ETL in OPVs with inverted structures because of their high carrier transport ability, transparency to visible light, stability, and ease of manufacturing. However, their stability and high-temperature processes

* Corresponding author.
E-mail address: dkmoon@konkuk.ac.kr (D.K. Moon).

https://doi.org/10.1016/j.jiec.2024.02.017
Received 31 October 2023; Received in revised form 12 January 2024; Accepted 9 February 2024
Available online 13 February 2024

hinder their modification. To solve this issue, dopants have been introduced into the ZnO layer, or additional layers have been formed on or under the ZnO layer.[29–32].

Quantum dots (QDs) have unique optoelectrical properties, which enable them to increase —upconversion (UC)—or decrease—downconversion (DC)—the wavelength of the incident light and amplify its intensity.[33–42] Thus, QDs have been used in various applications, such as, photodetector, light-emitting diodes (LEDs) and photovoltaics.[41,43–54] In particular, the light downconversion QDs that absorb ultraviolet (UV) light and emit visible light could contribute to photoactive layer absorbance and prevent photoactive material decomposition caused by high-energy UV light. Thus, the QDs can enhance the PCE and stability of an OPV.[52,54] Especially, zinc magnesium oxide (ZnMgO) QDs has great optical property that absorb light at 300 nm and emit light at 400–700 nm. And ZnMgO QDs has more stable property than that of other organic QDs. This nature could provide high performance and stability to OPV.

In this study, ZnMgO QDs was synthesized to obtain high performance OPVs via light downconversion. The photoactive layer of an OPV comprises a structured PM6 and a 2,2′-[[12,13-bis(2-butyloctyl)-12,13-dihydro-3,9-dinonylbisthieno-[2,″3:″4′,5′]thieno[2′,3′:4,5]-pyrrolo[3,2-e:2′,3′-g][2,1,3]-benzo-thiadiazole-2,10-diyl]bis[met-hylidyne(5,6-chloro-3-oxo-1H-indene-2,1(3H)-diylidene)]]bis-[propanedi-nitrile] (BTP-eC9) binary D/A system. The characteristics of the fabricated OPV devices were evaluated via various analyses.

Experimental section

Materials

Indium tin oxide (ITO) glass (sheet resistance, 10 Ω) was purchased from AMG (Korea). Zinc acetate dehydrate ($Zn(Ac)_2{\cdot}2H_2O$), magnesium acetate tetrahydrate ($Mg(Ac)_2{\cdot}4H_2O$), 2-methoxyethanol, chloroform (CF), dimethyl sulfoxide (DMSO), potassium hydroxide (KOH), acetone, ethyl alcohol (anhydrous) were purchased from Sigma-Aldrich (United states). PM6 and BTP-eC9 were purchased from Derthon (China). The additive 1,8-diiodooctane (DIO) was purchased from Alfa-Aesar (United states). The Ag electrode was prepared using Ag granules purchased from iTASCO (Korea).

Preparation for ZnMgO quantum dots solutions

DMSO (30 mL), $Zn(Ac)_2{\cdot}2H_2O$ (3 mmol), and $Mg(Ac)_2{\cdot}4H_2O$ (3 mmol) at a 9:1 ratio were added to a two-neck round-bottom flask equipped with a temperature-controllable hot plate. The mixture was stirred for 15 min at room temperature (RT) of 298 K. Simultaneously, KOH pellets (5 mmol) were dissolved in anhydrous ethyl alcohol (10 mL). The resulting KOH solution was added dropwise to the reaction mixture at 30 °C within 2 min. After 25 min, the mixture temperature was raised to 70 °C, and the mixture was immediately cooled to RT (298 K) using a water bath. The solution was washed and purified twice using an acetone/ethyl alcohol mixture and centrifuged to obtain a nanocrystal precipitate, which was redissolved in ethyl alcohol. Finally, the dispersion was centrifuged at 5,000 rpm for 4 min, the supernatant was collected, and the large particles were discarded.[55].

Device fabrication

The ITO glass (substrate) was sequentially washed with acetone, a detergent, isopropyl alcohol (IPA), and deionized water in an ultrasonicator. It was subsequently annealed and cleaned using a hot plate and a UV ozone cleaner, respectively. The ETL was cast on the ITO glass after its cleaning. A ZnO sol–gel solution was prepared from a mixture of zinc acetate, 2-methoxyethanol, and ethanolamine. Control ETL solution was prepared by mixing ZnO and ZnMgO at a volume ratio of 1:0.1. Both of ETL films were formed via spin coating under ambient conditions. The ETL formed was annealed for 1 h at 150 °C using a hot plate. Subsequently, a photoactive layer was formed using PM6 as the donor and BTP-eC9 as the acceptor at a mass ratio of 1:1.2 in a solution of CF (1,8-DIO, 0.5 vol%). The photoactive layer film was annealed after spin-coating the active material solution in a glove box. Next, the HTL MoO_3 and Ag electrodes, 5 and 100 nm in thickness, respectively, were formed via thermal deposition using a thermal evaporator under a pressure in the range from 10^{-6} to 10^{-7} torr.

Device characterization

The power conversion efficiencies and photovoltaic characteristics of the OPVs produced in this study were assessed using a Keithley 2400 source measure unit. A 1000 W Oriel solar simulator was used as the light source, and the intensity of incident light was set based on a reference silicon solar cell measured under AM 1.5 G irradiation (100 mW cm^{-2}), as per the suggestion of the National Renewable Energy Laboratory (NREL). The external quantum efficiencies (EQE) of the fabricated OPVs were measured using a Polaronix K3100 incident-photon-to-electron conversion efficiency (IPCE) measurement system, which allowed the measurement of the incident PCE. Atomic force microscopy (AFM) and electrostatic force microscopy (EFM) were performed using the PSIA XE-100 AFM, EFM instrument. High-resolution transmission electron microscope (HR-TEM, JEM-2100F) was used to analyze the particle diameters and lattice fringes of ZnMgO QDs. UV–visible (UV–vis) spectroscopy (Agilent 8453) and photoluminescence (PL) spectroscopy (Perkin Elmer LS-55) were used to analyze the absorbtion and emission properties of QDs.

Results and discussion

Properties of the photoactive layer and ETLs of the fabricated OPVs

Fig. 1 shows the molecular structures of the photoactive materials with (a) PM6 as the donor, (b) BTP-eC9 as the acceptor in the photoactive layer, (c) ZnO and ZnO:ZnMgO QDs solutions as the ETL (under UV light), and (d) the inverted structures of fabricated OPVs devices.

Optical characteristics of the fabricated OPVs

Fig. 2 shows the UV–vis absorbance and PL spectra data of the ETLs, whereas Fig. 2a shows the UV–vis absorbance and PL spectra of ZnMgO QDs film. As Fig. 2 shows, ZnMgO QDs absorb light at the wavelengths below 300 nm and emit light at the wavelengths range of 400–700 nm (λ_{max} @550 nm). Fig. 2b shows the PL spectra of the reference ETL film (ZnO) and ZnMgO QDs-doped ETL film (ZnO:ZnMgO QDs). The reference film shows a broad and weak ZnO PL intensity peak (λ @350–700 nm). After introducing ZnMgO QDs into ZnO, the PL intensity is significantly increased (λ @400–700 nm). The calculated photoluminescence quantum yield (PLQY) of the ZnMgO QDs was calculated 93.43 %. The PLQY was calculated using the following equation: $\Phi_{f,q} = \Phi_{f,r} \times m_q/m_r \times \eta_q^2/\eta_r^2$, where the $\Phi_{f,q}$ and $\Phi_{f,r}$ is the PLQYs of reference ETL and ZnMgO QDs-doped ETL, 'm' is the slope of the line obtained from the plot of absorbance vs. integrated PL intensity, and 'η' is the refractive index of the solvent.[36] This finding indicates that ZnMgO QDs convert UV light to visible light and emit amplified light to the photoactive layer, thereby enhancing the optoelectrical characteristics of the OPVs.

Photovoltaic characteristics of the fabricated OPVs

The photovoltaic characteristics of the fabricated OPVs are presented in Fig. 3 and Table 1. The reference device showed a PCE of 15.12 % (V_{OC} = 0.824 V, J_{SC} = 24.8 mA cm^{-2}, FF = 74.0 %). The PCE of the ZnMgO QDs device increased to 15.69 % (V_{OC} = 0.830 V, J_{SC} = 25.3 mA cm^{-2}, FF = 74.8 %). This enhancement mainly resulted in an increase in

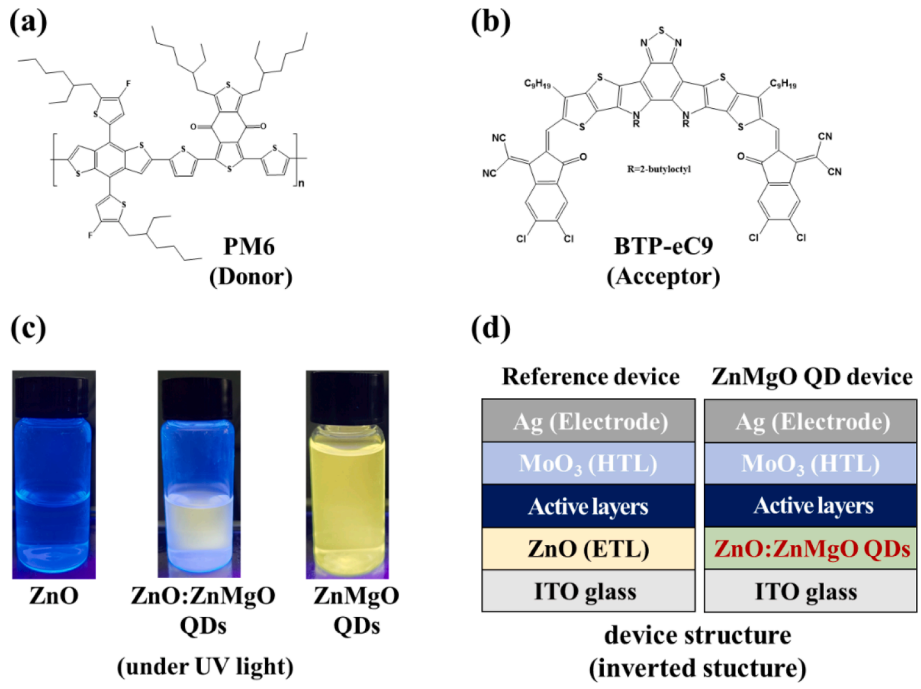

Fig. 1. Molecular structures of (a) PM6 as the donor, (b) BTP-eC9 as the acceptor, (c) images of ZnO, ZnO:ZnMgO QDs solutions as the ETL (under UV light), and (d) the inverted structures of fabricated OPVs devices.

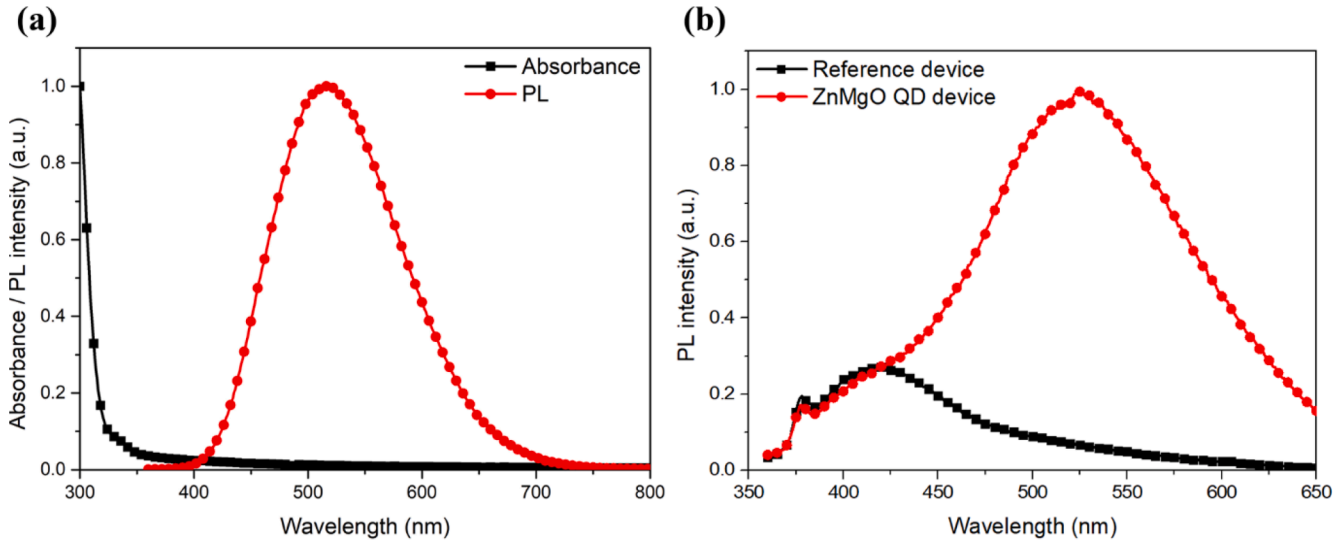

Fig. 2. Normalized UV–vis absorbance and PL spectra data of (a) ZnMgO QDs film, PL spectra data of (b) reference film and ZnO:ZnMgO QDs film.

J_{SC} and FF. The increased J_{SC} resulted from improved absorption of donor polymer. In Fig. 3b, the EQE (λ @400–700 nm) and calculated J_{SC} of the ZnMgO QDs device has higher than than those of the reference deivce. This result means that converted light from ZnMgO QDs was absorbed to donor and reinforced its electron withdrawing property. This result agrees with the UV–vis and PL spectroscopy results of the ETL, which indicates that the light conversion and amplification effects of the ZnMgO QDs increase the J_{SC} of the OPV device.

Fig. S1 shows the dark current density–voltage (*J–V*) characteristics of the reference and ZnMgO QDs devices. The *J-V* curves can be devided into three regions: regions I, II, and III. In the region I, which refers to the reverse bias region and front part of forward bias region, the *J-V* curve is mainly affected by shunt resistance (R_{sh}) of an OPV. In this region, the current density of the ZnMgO QDs device was lower than that of the reference device, implying that ZnMgO QDs device had a lower leakage current. In region II, the slope of the *J-V* curve turned sharply upward. The *J-V* curve of an OPV is determined by the diffusion and recombination currents. In region II, the current density of ZnMgO QDs device was higher than that of the reference device, implying that ZnMgO QDs device exhibited higher charge diffusion. In region III, the *J-V* curve was affected by the series resistance (R_s). In this region, an increase in R_s could lead to a reduction in the FF and PCE. The current density of the ZnMgO QDs device in region III is higher than that of the reference device making the charge transfer of the ZnMgO QDs device higher. Thus, the higher R_{sh} and lower R_s of the ZnMgO QDs device, as compared to those of the reference device, enhanced the FF and PCE of device.[56–59].

Fig. 4a and b show the dependence of the photocurrent density (J_{ph}) of the fabricated device on its effective voltage (V_{eff}) and exciton dissociation probability (P_{diss}). Fig. 4a shows the photocurrent densities

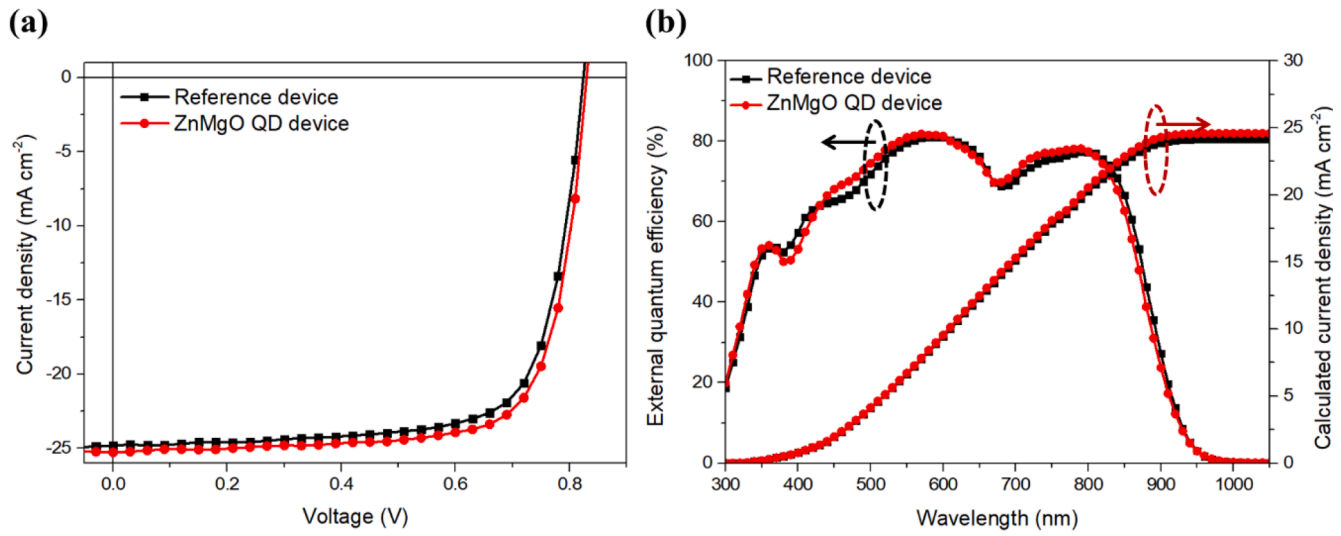

Fig. 3. (a) current density–voltage (J–V curve) characteristics under constant incident light intensity (AM 1.5G, 100 mW cm^{-2}) and (b) external quantum efficiency (EQE) characteristics of fabricated OPV devices with ETLs based on the photoactive layer PM6:BTP-eC9.

Table 1
Photovoltaic performance of fabricated OPV devices with ETLs based on PM6:BTP-eC9 after optimisation.[a]

Photoactive layer	Electron transport layer	V_{OC} (V)	J_{SC} (mA cm^{-2})	$J_{SC,\ cal}$ (mA cm^{-2})	FF (%)	PCE (%)
PM6:BTP-eC9	1. Reference ETL (ZnO)	0.824	24.8	24.16	74.0	15.12
	2. QDs-doped ETL (ZnO:ZnMgO QDs)	0.830	25.3	24.78	74.8	15.69

[a] Devices were fabricated with an inverted structure (ITO/ZnO/photoactive layer/HTLs/Ag, active area = 0.04 cm^2).

of the reference and ZnMgO QDs devices. The J_{ph}, V_{eff}, and J_{sat} of the devices were calculated using the following equations: $J_{ph} = J_L - J_D$, where J_L is the current density of the device under illumination and J_D is its current density under dark conditions, and $V_{eff} = V_0 - V$, where V is the applied voltage and V_0 is the compansation voltage at which $J_{ph} = 0$. The J_{ph} of the ZnMgO QDs device was higher than that of the reference device. The saturation current densities (J_{sat}) of the reference and ZnMgO QDs devices were measured at 0.5 V and 0.39 V, respectively. This higher J_{ph} and faster saturation of the ZnMgO QD device indicated better charge collection and extraction than the reference device. [23,60] Fig. 4b shows the exciton dissociation probability (P_{diss}) of the reference and ZnMgO QDs devices. The calculated P_{diss} values of the reference and ZnMgO QDs devices were 96.5 % and 97.9 %, respectively. This result agrees with EQE analysis results and dark J-V data.

Fig. S2 and Table S2 present the electron and hole moblilities (carrier mobility) of fabricated OPV devices, measured using the space-charge limit current (SCLC) method. We fabricated electron-only and hole-only devices to ensure electron and hole mobilities. The device structures were either ITO/ZnO or ZnO:ZnMgO QDs/photoactive layer/PDINN/Ag, and ITO/PEDOT:PSS/photoactive layer/MoO_3/Ag. The carrier mobilities of devices were calculated using the Mott-Gurney law. The calculated electron mobilities (μ_e) of the reference and ZnMgO QDs devices were 1.37 × 10^{-4} cm^2 V^{-1} s^{-1} and 1.53 × 10^{-4} cm^2 V^{-1} s^{-1},

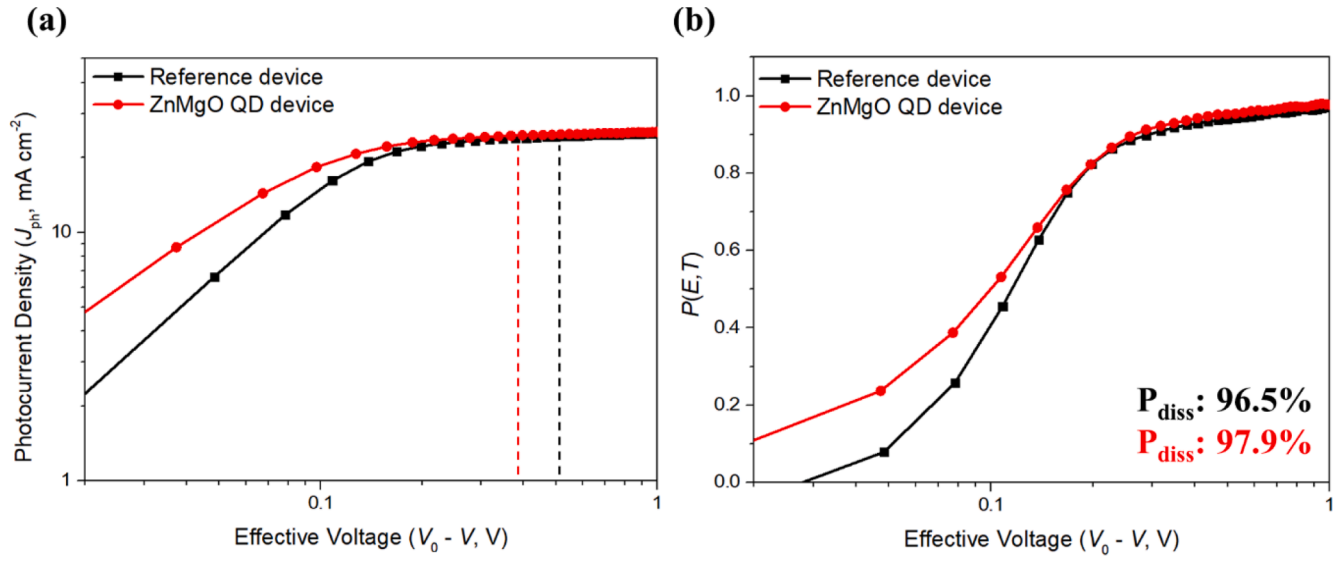

Fig. 4. (a) Dependence of photocurrent density (J_{ph}) on effective voltage (V_{eff}) and (b) exciton dissociation probability of fabricated device under constant incident light intensity (AM 1.5G, 100 mW cm^{-2}).

respectively. The calculated hole mobility (μ_h) of each device was 1.54 $\times$ 10^{-4} cm^2 V^{-1} s^{-1}. After introducing ZnMgO QDs into the ETL, its electron mobility increased significantly. The balance carrier (electron, hole) moblilities (μ_e/μ_h) of the reference and ZnMgO QDs devices obtained by calculation were 0.88 and 0.99, respectively. Thus the ZnMgO QDs have increased carrier transport and reduced carrier recombination. This result agrees with the UV, PL and EQE measurements.

Nanocrystal structure and surface morphology characteristics of the fabricated OPVs

Fig. 5a and b show the spherical HR-TEM images of the synthesized ZnMgO QDs and their lattice fringes. The Bohr radius of the ZnO and MgO were 2.34 nm and 1.6 nm, respectively. The calculated average diameter of the ZnMgO QDs was approximately 5.19 nm, and its average lattice spacing was 0.307 nm. The measured diameter of the ZnMgO QDs was similar to the sum of the Bohr radius, and the lattice spacing between any two molecules was similar to that of the (002) plane of wurtzite ZnO.[55,61] Fig. 5c presents selected area electron diffraction (SAED) pattern of the ZnMgO QDs. Distinct ring patterns corresponding to the (100), (002), and (101) planes of the ZnO wurtzite structure and the (220) and (200) planes of the MgO structure can be observed in the SAED image. Thus, the ZnO and MgO nanocrystals are present in the ZnMgO QDs.[62] Fig. 5d presents the histogram distribution of the synthesized ZnMgO QDs with different diameters.

Fig. S3a-d present the surface morphologies and potential data of the reference and ZnMgO QDs-doped films obtained using AFM and EFM analyses. Fig. S3a and b show the two-dimensional AFM topography images of the two films. The measured RMS roughness (R_q) values of the reference and ZnMgO QDs films were 0.818 nm and 0.819 nm, respectively. Thus, despite the introducion of additional dopants (ZnMgO QDs) to the ZnO film, the surface morphology of the ETL had not changed or aggravated. Fig. S3c and d show the EFM amplitude data of the reference and ZnMgO QDs films. The measured surface potential (R_{mean}) of the reference and ZnMgO QDs films were 480.473 mV and 459.824 mV, respectively. After the introducion of the ZnMgO QDs to the ETL, its R_{mean} decreased. A lower R_{mean} indicates that ZnMgO QDs forms an appropriate electric field in the inverted structures of the OPV.[63,64] This electric field modification could significantly enhance the J_{SC} and FF of the OPV device.

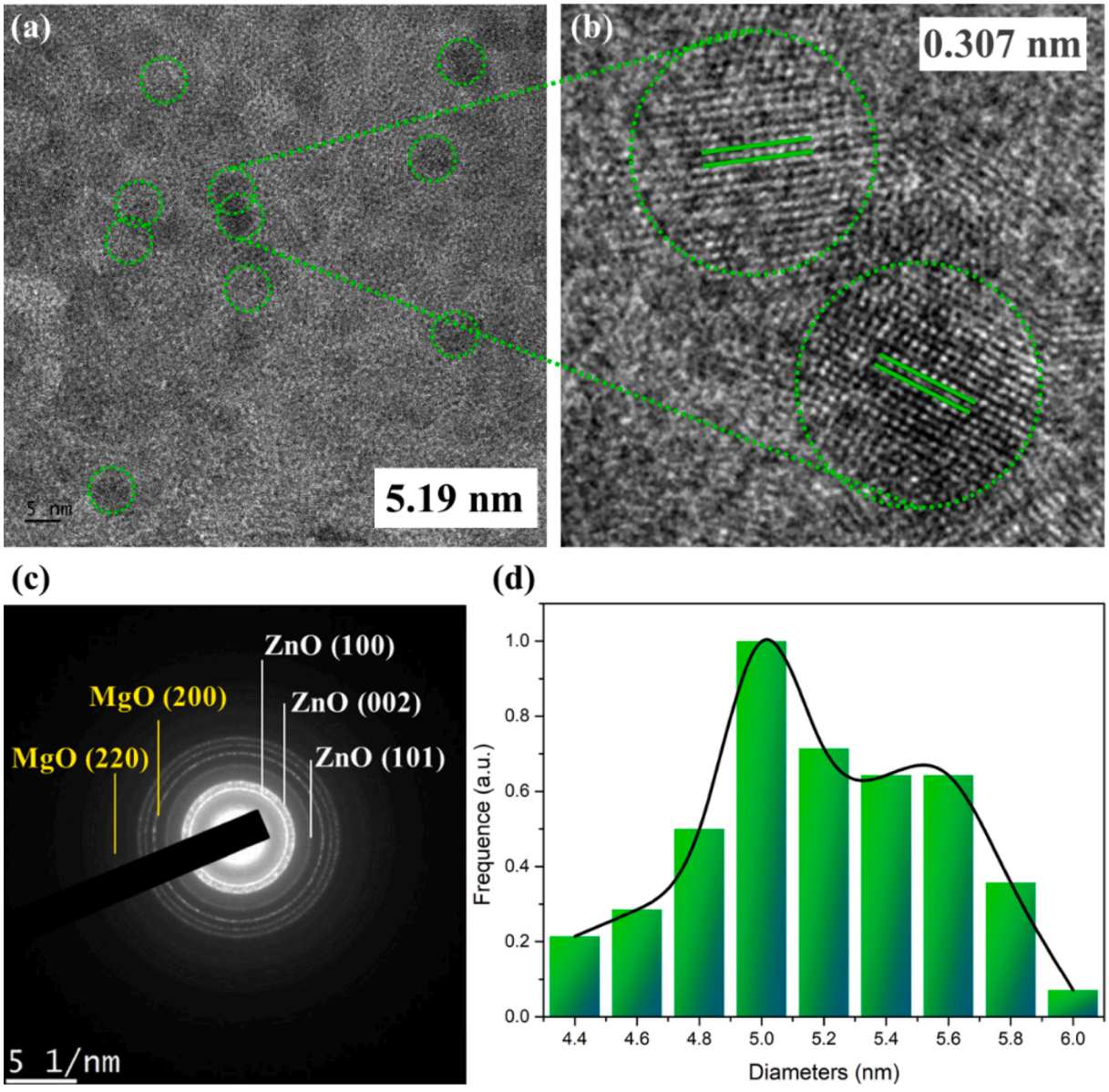

Fig. 5. HR-TEM image of (a) 5 nm scale, (b) 2 nm scale and (c) image of selected area electron diffraction (SAED), (d) histogram distribution of diameter size.

Conclusions

In this study, we introduced ZnMgO QDs that can downconvert UV for use as an ETL in OPVs that have BHJ-structured PM6/BTP-eC9 as photoactive layers.

Recently, several studies have been conducted on the use of QDs in the development of high-performance OPVs. QDs have unique optical properties, such as light conversion ability, enabling it to absorb and emit light after changing its wavelength. Because of these properties, QDs have been introduced into the active layers or interlayers of OPVs.

The UV–vis and PL measurements showed that the ZnMgO QDs absorbed 300 nm light and emitted light with wavelengths in the range of 400–700 nm. Furthermore, the EQE of the ZnMgO QDs device increased between 400 and 700 nm. Thus, the ZnMgO QDs contributed to the absorbance of the donor.

The fabricated OPVs with ZnMgO QDs as the ETL demonstrated a higher J_{SC} (25.3 mA cm^{-2}) than the reference device (24.8 mA cm^{-2}). Thus, PCE was increased from 15.12 % to 15.69 %. These results suggest that visible-light-emitting QDs contribute to the fabrication of high-performance and semi-transparent OPV devices and modules.

CRediT authorship contribution statement

Hyoung Seok Lee: Conceptualization, Data curation, Writing – original draft, Writing – review & editing, Visualization, Investigation, Validation, Formal analysis, Methodology. **Chang Ho Jung:** Writing – review & editing, Investigation. **Doo Kyung Moon:** Funding acquisition, Supervision, Resources, Project administration, Software.

Declaration of competing interest

The authors declare that they have no known competing financial interests or personal relationships that could have appeared to influence the work reported in this paper.

Acknowledgements

This research was supported by Konkuk University, South Korea in 2021.

Appendix A. Supplementary data

Supplementary data to this article can be found online at https://doi.org/10.1016/j.jiec.2024.02.017.

References

[1] R. Jyoti, Deji, M. Chauhan, B.C. Choudhary, R.K. Sharma, ES Energy Environ. 18 (2022) 47–55. 10.30919/esee8c701.
[2] S. Zheng, M. Zhang, M. Na, Y. Yang, Z. Luo, Q. Lu, ES Energy Environ. 17 (2022) 33–43. 10.30919/esee8c635.
[3] S.P. Gupta, P.P. Sanap, G. V. Dilwale, R.N. Bulakhe, A.D. Jagadale, M.K. Deore, A. B. Bhalerao, C.D. Lokhande, ES Energy Environ. 20 (2023) 1–7. 10.30919/esee910.
[4] M. Sadullah, K. Ghosh, ES Energy Environ. 20 (2023) 1–9. 10.30919/esee883.
[5] P. Sabbaghi, Q. Ni, L. Wang, ES Energy Environ. 18 (2022) 56–64. 10.30919/esee8c752.
[6] J. Kaur, H.D. Shelke, S.R. Jadkar, H.M. Pathan, R. Kumar, ES Energy Environ. 17 (2022) 56–63. 10.30919/esee8c743.
[7] J. Huang, J. Zhou, E. Jungstedt, A. Samanta, J. Linnros, L.A. Berglund, I. Sychugov, ACS Photonics 9 (7) (2022) 2499–2509, https://doi.org/10.1021/acsphotonics.2c00633.
[8] M. Bates, C. Malhado, C. Yang, C.K. Herrera, R.R. Lunt, Sol. RRL 7 (10) (2023) 1–11, https://doi.org/10.1002/solr.202200962.
[9] E.K. Solak, E. Irmak, RSC Adv. 13 (18) (2023) 12244–12269, https://doi.org/10.1039/d3ra01454a.
[10] G.P. Kini, S.J. Jeon, D.K. Moon, Adv. Funct. Mater. 31 (2021) 15, https://doi.org/10.1002/adfm.202007931.
[11] J. Wu, ES Energy Environ. 15 (2022) 76–81. 10.30919/esee8c619.
[12] Y. Zhong, D. Liu, Q. Yang, Y. Qu, C. Yu, K. Yan, P. Xie, X. Qi, Z. Guo, Z. Toktarbay, Eng. Sci. (2023) 1–12, https://doi.org/10.30919/es988.
[13] D. Bhargava, P. Rattanadecho, Eng. Sci. 21 (2023) 1–12. 10.30919/es8d796.
[14] C. An, Z. Zheng, J. Hou, Chem. Commun. 56 (35) (2020) 4750–4760, https://doi.org/10.1039/d0cc01038c.
[15] A. Karki, A.J. Gillett, R.H. Friend, T.Q. Nguyen, Adv. Energy Mater. 11 (15) (2021) 1–30, https://doi.org/10.1002/aenm.202003441.
[16] S.J. Jeon, Y.H. Kim, I.N. Kim, N.G. Yang, J.H. Yun, D.K. Moon, J. Energy Chem. 65 (2022) 194–204, https://doi.org/10.1016/j.jechem.2021.05.032.
[17] N.G. Yang, S.J. Jeon, Y.H. Kim, H.S. Lee, D.H. Hong, D.K. Moon, J. Ind. Eng. Chem. 112 (2022) 76–84, https://doi.org/10.1016/j.jiec.2022.05.001.
[18] G.P. Kini, Y.W. Han, S.J. Jeon, E.J. Lee, Y.J. Lee, M. Goh, D.K. Moon, Macromol. Rapid Commun. 43 (15) (2022) 1–10, https://doi.org/10.1002/marc.202200070.
[19] S.J. Jeon, N.G. Yang, Y.H. Kim, J.H. Yun, D.K. Moon, ACS Appl. Mater. Interfaces 14 (33) (2022) 38031–38047, https://doi.org/10.1021/acsami.2c10286.
[20] S.J. Jeon, Y.C. Kim, J.Y. Kim, J.H. Kim, N.G. Yang, Y.J. Lee, H.S. Lee, Y.H. Kim, G. W. Kim, E.M. Jang, B.K. Lee, C. Yang, D.K. Moon, Chem. Eng. J. 472 (June) (2023) 144850, https://doi.org/10.1016/j.cej.2023.144850.
[21] S.J. Jeon, N.G. Yang, J.Y. Kim, Y.C. Kim, H.S. Lee, D.K. Moon, Small 2301803 (2023) 1–11, https://doi.org/10.1002/smll.202301803.
[22] Z. Peng, Y. Zhang, X. Sun, W. Zhao, F. Bian, Y. Geng, L. Ye, C. Yang, Adv. Funct. Mater. 33 (2023) 14, https://doi.org/10.1002/adfm.202213248.
[23] Y. Wang, W. Xu, J. Yi, C. Zuo, Y. Gong, Y. Liu, W.Y. Lai, W. Huang, J. Mater. Chem. A 6 (33) (2018) 15977–15984, https://doi.org/10.1039/c8ta03043j.
[24] M. Zhang, X. Guo, W. Ma, H. Ade, J. Hou, Adv. Mater. 27 (31) (2015) 4655–4660, https://doi.org/10.1002/adma.201502110.
[25] J. Yuan, Y. Zhang, L. Zhou, G. Zhang, H.L. Yip, T.K. Lau, X. Lu, C. Zhu, H. Peng, P. A. Johnson, M. Leclerc, Y. Cao, J. Ulanski, Y. Li, Y. Zou, Joule 3 (4) (2019) 1140–1151, https://doi.org/10.1016/j.joule.2019.01.004.
[26] C. Han, J. Wang, S. Zhang, L. Chen, F. Bi, J. Wang, C. Yang, P. Wang, Y. Li, X. Bao, Adv. Mater. 35 (10) (2023) 1–13, https://doi.org/10.1002/adma.202208986.
[27] M. Deng, X. Xu, Y. Duan, L. Yu, R. Li, Q. Peng, Adv. Mater. 35 (10) (2023) 1–10, https://doi.org/10.1002/adma.202210760.
[28] Y.W. Han, H.S. Lee, D.K. Moon, ACS Appl. Mater. Interfaces 13 (16) (2021) 19085–19098, https://doi.org/10.1021/acsami.1c01021.
[29] W.C.H. Choy, D. Zhang, Small 12 (4) (2016) 416–431, https://doi.org/10.1002/smll.201502258.
[30] Y. Wang, Q. Chen, G. Zhang, Y. Wang, Z. Zhang, J. Fang, C. Zhao, W. Li, Chem. Eng. J. 451 (P1) (2023) 138612, https://doi.org/10.1016/j.cej.2022.138612.
[31] R.D. Chavan, M. Wolska-Pietkiewicz, D. Prochowicz, M. Jędrzejewska, M. M. Tavakoli, P. Yadav, C.K. Hong, J. Lewiński, Adv. Funct. Mater. 32 (2022) 49, https://doi.org/10.1002/adfm.202205909.
[32] Alamgeer, M. Tahir, M.R. Sarker, S. Ali, Ibraheem, S. Hussian, S. Ali, M. Imran Khan, D.N. Khan, R. Ali, S. Mohd Said, Polymers (Basel). 15(2) (2023). 10.3390/polym15020363.
[33] D. Petris, D.V. Freitas, R.K.V. Dos Santos, J.M.M. Dias, M. Navarro, Mater. Res. Express 4 (7) (2017), https://doi.org/10.1088/2053-1591/aa7e03.
[34] X. Ren, L. Pang, Y. Zhang, X. Ren, H. Fan, S. Liu, J. Mater. Chem. A 3 (20) (2015) 10693–10697, https://doi.org/10.1039/c5ta02198g.
[35] V. Cilamkoti, R.K. Dutta, J. Photochem. Photobiol. A Chem. 436(October 2022) (2023) 114406. 10.1016/j.jphotochem.2022.114406.
[36] D. Kandi, S. Mansingh, A. Behera, K. Parida, J. Lumin. 231(November 2020) (2021) 117792. 10.1016/j.jlumin.2020.117792.
[37] Z. Song, Z. Zheng, Y. Zhang, X. Cao, S. Li, H. Zhang, C. Luo, Y. Li, X. Zhang, J. Lumin. 256(December 2022) (2023) 119622. 10.1016/j.jlumin.2022.119622.
[38] S. Akhil, J. Kusuma, R.G. Balakrishna, J. Clean. Prod. 366 (June) (2022) 132760, https://doi.org/10.1016/j.jclepro.2022.132760.
[39] E.P. Jang, C.Y. Han, S.W. Lim, J.H. Jo, D.Y. Jo, S.H. Lee, S.Y. Yoon, H. Yang, ACS Appl. Mater. Interfaces 11 (49) (2019) 46062–46069, https://doi.org/10.1021/acsami.9b14763.
[40] M. Fujii, R. Fujii, M. Takada, H. Sugimoto, ACS Appl. Nano Mater. 3 (6) (2020) 6099–6107, https://doi.org/10.1021/acsanm.0c01295.
[41] Z. Liang, Y. Chen, R. Zhang, K. Zhang, K. Ba, Y. Lin, D. Wang, T. Xie, Dalt. Trans. 51 (45) (2022) 17292–17300, https://doi.org/10.1039/d2dt02555h.
[42] X. Chen, Q. Wang, X.J. Wang, J. Li, G. Bin Xu, Sci. Rep. 11(1) (2021) 1–9. 10.1038/s41598-021-85468-z.
[43] J.E. Alassafi, Y. Al-Hadeethi, M. Saleh Aida, S. Fayez Al-Shehri, M. Chen, Eng. Sci. 1–14 (2023), https://doi.org/10.30919/es986.
[44] H.S. Yang, D. Lee, E.H. Suh, S.H. Noh, K.H. Lee, J.G. Oh, J. Jung, J. Jang, Chem. Eng. J. 457(December 2022) (2023) 141107. 10.1016/j.cej.2022.141107.
[45] R. Kottayi, V. Ilangovan, R. Sittaramane, Opt. Mater. (Amst) 134 (PA) (2022) 113036, https://doi.org/10.1016/j.optmat.2022.113036.
[46] S.D. Baek, D.K. Kwon, Y.C. Kim, J.M. Myoung, ACS Appl. Mater. Interfaces 12 (5) (2020) 6037–6047, https://doi.org/10.1021/acsami.9b18507.
[47] R. Kottayi, D.K. Maurya, R. Sittaramane, S. Angaiah, ES Energy Environ. 18 (2022) 1–40. 10.30919/esee8c754.
[48] F.A. Al-Marhaby, M.S. Al-Ghamdi, A. Zekry, Eng. Sci. 18 (2022) 132–40. 10.30919/es8d647.
[49] H. Algadi, T. Das, J. Ren, H. Li, Adv. Compos. Hybrid Mater. 6 (2023) 2, https://doi.org/10.1007/s42114-023-00634-3.
[50] J. Liu, J. Wang, Y. Liu, K. Xian, K. Zhou, J. Wu, S. Li, W. Zhao, Z. Zhou, L. Ye, J. Mater. Chem. A 11 (3) (2022) 1013–1038, https://doi.org/10.1039/d2ta07671c.
[51] J.H. Kim, Y.C. Kim, J.Y. Kim, H.S. Lee, Y.W. Han, H.W. Lee, D.K. Moon, 2300057, Small Struct. (2023) 1–13, https://doi.org/10.1002/sstr.202300057.
[52] Y.W. Han, C.H. Jung, H.S. Lee, S.J. Jeon, D.K. Moon, ACS Appl. Mater. Interfaces 12 (34) (2020) 38470–38482, https://doi.org/10.1021/acsami.0c09539.
[53] T. Chiba, J. Kido, J. Mater. Chem. C 6 (44) (2018) 11868–11877, https://doi.org/10.1039/c8tc03561j.

[54] Y.W. Han, S.J. Jeon, J.Y. Choi, J.H. Kim, D.K. Moon, Sol. RRL 2 (9) (2018) 1–11, https://doi.org/10.1002/solr.201800077.
[55] A. Saha, G. Kumar, S. Pradhan, G. Dash, R. Viswanatha, G. Konstantatos, Adv. Mater. 34 (10) (2022) 1–8, https://doi.org/10.1002/adma.202109498.
[56] M.H. Jao, H.C. Liao, W.F. Su, J. Mater. Chem. A 4 (16) (2016) 5784–5801, https://doi.org/10.1039/c6ta00126b.
[57] J.D. Servaites, M.A. Ratner, T.J. Marks, Energy Environ. Sci. 4 (11) (2011) 4410–4422, https://doi.org/10.1039/c1ee01663f.
[58] Y. Ma, H. Zhang, Y. Zhang, R. Hu, M. Jiang, R. Zhang, H. Lv, J. Tian, L. Chu, J. Zhang, Q. Xue, H.L. Yip, R. Xia, X. Li, W. Huang, ACS Appl. Mater. Interfaces 11 (3) (2019) 3044–3052, https://doi.org/10.1021/acsami.8b18867.
[59] P. Liao, X. Zhao, G. Li, Y. Shen, M. Wang, Nano-Micro Lett. 10 (1) (2018) 1–8, https://doi.org/10.1007/s40820-017-0159-z.
[60] J. De Chen, C. Cui, Y.Q. Li, L. Zhou, Q.D. Ou, C. Li, Y. Li, J.X. Tang, Adv. Mater. 27 (6) (2015) 1035–1041, https://doi.org/10.1002/adma.201404535.
[61] S. Baruah, C. Thanachayanont, J. Dutta, Sci. Technol. Adv. Mater. 9 (2008) 2, https://doi.org/10.1088/1468-6996/9/2/025009.
[62] C. Abed, M. Ben Ali, A. Addad, H. Elhouichet, Mater. Res. Bull. 110(September 2018) (2019) 230–8. 10.1016/j.materresbull.2018.10.041.
[63] Z. He, C. Zhong, X. Huang, W.Y. Wong, H. Wu, L. Chen, S. Su, Y. Cao, Adv. Mater. 23 (40) (2011) 4636–4643, https://doi.org/10.1002/adma.201103006.
[64] Y.W. Han, J.Y. Choi, Y.J. Lee, E.J. Ko, M.H. Choi, I.S. Suh, D.K. Moon, Adv. Mater. Interfaces 6 (3) (2019) 1–15, https://doi.org/10.1002/admi.201801396.